

NB-IoT over Non-Terrestrial Networks: Link Budget Analysis

Matteo Conti*, Alessandro Guidotti*, Carla Amatetti*, and Alessandro Vanelli-Coralli*

*Department of Electrical, Electronic, and Information Engineering (DEI), University of Bologna, Bologna, Italy

Abstract—Machine Type Communications (MTC) and Internet of Things (IoT) applications are growing exponentially and are forecast to play an even more important role in Future Networks and Systems. The Third Generation Partnership Project (3GPP) introduced the Narrowband IoT (NB-IoT) air interface as a response to the IoT use case requirements. However, it is widely accepted that the terrestrial network alone is not able to serve the requirement of the IoT market of a truly ubiquitous coverage. To this aim, several initiatives are currently addressing the inclusion of a satellite component into the telecommunication infrastructure to extend its coverage to those areas that are unserved or underserved by the terrestrial network. The recently approved 3GPP study item on *NB-IoT over Non-Terrestrial Network (NTN)* is the most important of these initiatives. The study item, starting at the beginning of 2021, will assess the performance of the NB-IoT air interface over satellite and will identify which adaptations are needed to enable its use. In this context, our work provides an assessment of the system level performance, in terms of the link budget parameters, of the NB-IoT air interface in typical satellite scenarios. In particular, we provide a detailed discussion of the system architecture supporting the NB-IoT over NTN, a description of the link budget computation methodology, and the numerical results of the link budget analysis in both single-satellite and multi-satellite scenarios.

Index Terms—NB-IoT, Satellite Communications, Link Budget, Non-Terrestrial Networks, Internet of Things.

I. INTRODUCTION

In recent years, Internet of Things (IoT) applications have drawn a great deal of attention, both in academia and industry. It is, in fact, expected that IoT devices will be half of the global connected devices within the next few years, with 14.7 billion Machine to Machine (M2M) connections by 2023 [1]. A crucial requirement of any infrastructure serving the IoT market will be to guarantee ubiquitous connectivity to the low-cost, low-powered devices distributed all over the globe. It is widely accepted that this requirement will not be met by the terrestrial network alone. There will be, in fact, vast areas of the globe where the terrestrial infrastructure deployment will be unfeasible or not economically viable, thus leaving those areas un- or under-served. For this reason, several studies are addressing the use of a Non-Terrestrial Network (NTN) component to seamlessly complement and extend the terrestrial network coverage in future systems [2]–[6] and the Third Generation Partnership Project (3GPP) decided to study the feasibility of using the Narrowband IoT (NB-IoT) air-interface over the NTN in its release 17 [7]. The study phase, starting in 2021, will identify the needed adaptations and assess the performance of NB-IoT over NTN.

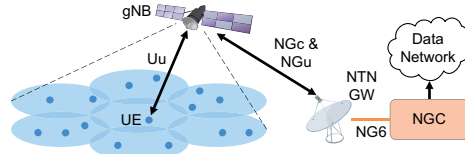


Fig. 1: High-level system architecture: access based on regenerative payload.

In this framework, several scientific works have been published on the subject. An overview of the possible challenges of NB-IoT over NTN is reported in [8]. The effects of the high *Doppler* and *delay* induced by non-geostationary satellites and the possible countermeasures are elaborated in details in [9]–[11]. The design of a NB-IoT receiver in the presence of Doppler effects, at the Gateway (GW) side, is addressed in [12]. An initial interesting analysis of the *link budget* is presented in [13], where the case of a single satellite, in Low Earth Orbit (LEO) at a given elevation angle, is addressed to shed light on the trade-offs between the link parameters and the payload characteristics.

However, to fully support the system design of future NB-IoT over NTN, the link budget analysis shall consider the NTN architecture in its entire complexity, in particular it shall address the effect of moving non-geostationary satellites, *i.e.*, different elevation angles, actual propagation conditions, and multi-beam and multi-user interference. This paper presents this analysis.

In the following, we provide the link budget evaluation for an NB-IoT systems by considering fixed IoT device on Earth and moving LEO satellites in different constellations, accounting for the multi-beam interference, in the down-link, and the multi-user interference, in the up-link. In doing this, we discuss the NTN system architecture options currently considered within 3GPP and the system assumptions, and we perform a link budget calibration in both the down-link and the up-link according to [14], [15] by extending to NB-IoT the work reported in [16].

II. SYSTEM MODEL

A. Architecture

With reference to Fig. 1, the main elements of the high level system architecture [15] are: *i*) a User Equipment (UE), which is a NB-IoT device, fixed or mobile; *ii*) a regenerative payload satellite or Unmanned Aircraft System (UAS), providing connectivity to the UE through the user link; *iii*) a gNB implemented on the satellite; *iv*) a ground segment GW

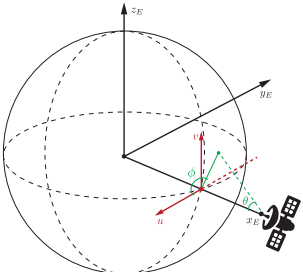


Fig. 2: Reference system for antenna pattern computations.

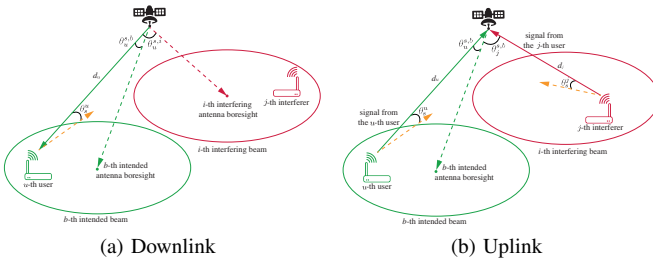


Fig. 3: Geometry for link budget computation.

interconnected to the flying platform through the feeder link; v) the Next Generation Core network (NGC).

The aforementioned architecture can be declined into different scenarios, [14], depending on the orbit and altitude of the flying platforms. In the first stage of standardization for NTN, the focus is on Geostationary Orbit (GEO) platforms and LEO platforms at 600 and 1200 km of altitude. For LEO platforms, the coverage can be achieved with *fixed* or *moving* beams. In the former case, the on-board antenna keeps serving the same on-ground area while the satellite moves on its orbit (steerable antennas). In the latter case, the served on-ground area is moving together with the satellite. Later in this paper, if not otherwise specified, we assume the following system configuration: direct access, regenerative payload, LEO or GEO multi-beam platform operating in S-band, with moving beams for LEO constellations. This configuration refers to scenario B and scenario D2 in [14].

B. Single- and Multi-Satellite Scenarios

For the Single-Satellite (S-S) scenario, the coverage area of the satellite, thus the multi-beam layout, are defined in $u-v$ coordinates. These two unit vectors are the direction cosines corresponding to the θ and ϕ of the Field Of View (FOV) from the satellite antenna, as depicted in the Fig. 2. Once the coordinates system for the satellite FOV is chosen, it is possible to define the hexagonal tessellation for a given transmitting antenna configuration and, thus, radiation pattern. Assuming θ_{3dB} as the antenna 3 dB angle, the beam radius on the $u-v$ plane is defined as $R_{3dB} = \sin(\theta_{3dB})$. The hexagonal tessellation on the $u-v$ plane is then obtained by locating the adjacent beam centers at a distance corresponding to the Adjacent Beam Spacing, $ABS = R_{3dB}\sqrt{3} = \sqrt{3}\sin(\theta_{3dB})$, as it is explained in [14], [16]. An example of satellite antenna pattern, with hexagonal tessellation is represented in Fig. 4. In [14], the values of ABS for LEO and GEO systems,

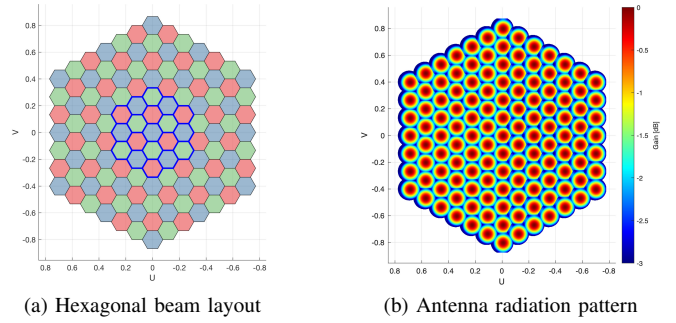


Fig. 4: Example of coverage ($u-v$ coordinates): LEO system in S-band; $h_{sat} = 1200$ km; FR3; 6 tiers (127 beams).

are provided assuming for the satellite antennas the Bessel radiation pattern of [15]. On the other hand, for the UE an omnidirectional antenna has been considered. It is worth highlighting that the antenna pattern described in [15] is defined regular with respect to $\theta-\phi$ coordinates, while the beam spacing is defined regular with respect to $u-v$ coordinates, i.e., circular beams with radius R_{3dB} are considered in [14]. This choice leads to a mismatch, in fact a regular grid in $\theta-\phi$ plane cannot be regular on the $u-v$ plane and viceversa. Therefore moving away from the central beam of the coverage, the surrounding beams begin to deform from the circular shape, leading to an imperfect coverage. However in this work we use a perfect coverage as initially intended from 3GPP documentation.

For the Multi-Satellite (M-S) scenario, the methodologies proposed in [14] and [17] have been taken into account. In particular we focus on the *Option-1*, for simulation based on a reference constellation, defining the parameters, e.g., number of orbits/satellites, number of beams. The detailed parameters can be determined jointly with consideration on the Radio Frequency (RF) characteristic of beams together with design principle for constellation, e.g., how to achieve global coverage. Considering a specific satellite, with a specific altitude and position, and referring to the beam layout previously defined, it is possible to derive the coverage on the Earth surface for that flying platform, thus the coverage for the entire constellation. Obtaining the projection from $u-v$ to Earth-Centered Earth-Fixed (ECEF) coordinates (x_E, y_E, z_E in Fig. 2) and latitude-longitude (*lat-lon*) coordinates is not trivial, but is out of the scope of this work. However it is worth highlighting that for this purpose, in the satellite coordinate reference system, the u -axis is pointing towards West and consequently the v -axis is pointing towards North. Then the values for the antenna pattern for each satellite in the constellation are projected in *lat-lon* coordinates, according to projection angles computed as described in [18].

III. LINK BUDGET

In the following, on the basis of [14], [15] and [16], we discuss the evaluation methodology for the link budget in DL and UL.

A. Losses

The overall path loss is defined as, [14], [15]:

$$PL = PL_{fs} + PL_\sigma + PL_{cl} + PL_{atm} + PL_s \quad (1)$$

with: PL_{fs} the free space loss; PL_σ the shadowing loss; PL_{cl} the clutter loss; PL_{atm} the losses due to atmospheric gases; and PL_s the signal loss due to tropospheric or ionospheric scintillations. A detailed description of the path loss components has been given in [16], however it is worth highlighting that: *i*) the UE is assumed always in Line of Sight (LoS) conditions and, thus, PL_{cl} is always zero; *ii*) the shadowing loss, PL_σ is modelled as a lognormal random variable with zero mean and a variance related to the harshness of the shadowing environment, *i.e.*, $PL_\sigma \sim (0, \sigma_s^2)$, and the values of, σ_s^2 are provided by 3GPP for dense urban, urban, and rural scenarios as a function of the elevation angle in [15]; *iii*) the term PL_{atm} taking into account the atmospheric losses is computed as provided in Annex 2 of ITU-R P.676 for slant paths; *iv*) the ionospheric scintillations, impacting signals in S-band, are modelled as a fixed term of 2.2 dB as from [15], and described in ITU-R P.531-13. Moreover ionospheric scintillations loss is not considered for calibration purposes in the S-S scenario as from [14]. Finally, tropospheric scintillations are not considered in S-band [15].

B. Downlink

For the DL computation, the reference scheme is shown in Fig. 3a, where: *i*) the intended u -th user is randomly located inside the intended b -th beam; *ii*) an interfering signal is transmitted from the i -th antenna towards the j -th user of the i -th beam; *iii*) d_u is the slant range of the u -th user in the b -th beam; *iv*) $\theta_u^{s,i}$ denotes the angle between the i -th antenna boresight of the s -th satellite, and the direction of the u -th user in the b -th beam (when $i = b$, this is the angle from the intended antenna boresight); *v*) θ_s^u denotes the angle between the antenna pointing of the u -th user and the s -th satellite, which does not depend on the satellite antenna index since they are assumed to be colocated. The intended power received by the u -th user in the b -th beam is given by:

$$C_u^{(DL)} = EIRP(\theta_u^{s,b}) + G_{RX}(\theta_s^u) - PL_u^s \quad (2)$$

where $G_{RX}(\theta_s^u)$ is the receiving UE antenna gain as a function of the angle between the UE antenna pointing and the s -th satellite direction; this value depends on the antenna pattern chosen for the UE, for the purpose of this work the UE antenna is considered omnidirectional. $EIRP(\theta_u^{s,b})$ is the transmitted Equivalent Isotropically Radiated Power from the intended b -th antenna, of the s -th intended satellite, towards the u -th user; and PL_u^s is the path loss for the u -th intended user with respect to the intended s -th satellite computed as in Eq. 1. The transmitted EIRP is computed as:

$$EIRP(\theta_u^{s,b}) = EIRP_{max}^{(DL)} + 10 \log_{10} \Omega(\theta_u^{s,b}) \quad (3)$$

where $EIRP_{max}^{(DL)} = \delta_{EIRP} + 10 \log_{10} B$ is the maximum EIRP, *i.e.*, the EIRP in the antenna boresight direction, with

δ_{EIRP} being the EIRP density, B the user bandwidth, which varies according to the Frequency Reuse (FR) scheme used. In the above formula, the radiation pattern of the satellite antenna $\Omega(\cdot)$ depends on the Bessel function in [15], as previously mentioned. The noise power at the receiver is independent of the UE, *i.e.*, it is the same $\forall u, b$, and it can be computed as follows:

$$N^{(DL)} = N_f + 10 \log_{10} (T_a - T_0) \cdot 10^{-0.1N_f} \cdot \kappa B \quad (4)$$

where N_f is the receiver noise figure, T_a is the receiver antenna temperature, κ is the Boltzmann constant, and $T_0 = 290$ K is the reference noise temperature. The Carrier-to-Noise Ratio (CNR), $CNR_u^{(DL)}$, is then obtained by subtracting Eq. 4 from Eq. 2. Finally, the overall interference at the u -th user in the b -th beam is given by:

$$I_u^{(DL)} = 10 \log_{10} \left(\sum_{k=1}^{N_{sat}} \sum_{i=1}^{N_{int}} 10^{0.1I_{k,i,u}^{(DL)}} \right) \quad (5)$$

where:

$$I_{k,i,u}^{(DL)} = EIRP(\theta_u^{k,i}) + G_{RX}(\theta_k^u) - PL_u^k \quad (6)$$

is the interference from the i -th interfering beam of the k -th satellite, with $i = 1, \dots, N_{int}$, and $k = 1, \dots, N_{sat}$; N_{int} being the number of co-channel beams and N_{sat} the number of satellite in the constellation. It shall be noticed that, in the i -th interference term, the satellite EIRP is now computed based on the angle between the i -th interfering antenna boresight and the direction of the u -th intended user in the b -th beam. From Eq. 5, it is straightforward to obtain the Carrier-to-Interference Ratio (CIR), $CIR_u^{(DL)}$, by subtracting Eq. 5 from Eq. 2. The overall Carrier-to-Interference plus Noise Ratio (CINR) is given by:

$$CINR_u^{(DL)} = -10 \log_{10} \left(10^{-0.1CNR_u^{(DL)}} + 10^{-0.1CIR_u^{(DL)}} \right) \quad (7)$$

It is worthwhile highlighting that the above formulation for the DL performance can be applied to any of the systems foreseen for NTN.

C. Uplink

For the UL, the reference scenario is depicted in Fig. 3b, where, in addition to the nomenclature introduced for the DL, are shown: *i*) the interfering j -th user is randomly located inside the interfering i -th beam; *ii*) d_j is the slant range of the j -th user in the i -th beam; *iii*) $\theta_j^{s,b}$ denotes the angle between the intended receiving b -th antenna boresight and the direction of arrival of the interfering signal from the j -th user in the i -th beam; *iv*) θ_s^j denotes the angle between the antenna pointing of the j -th user in the i -th beam and the s -th satellite, which does not depend on the satellite antenna index due to antenna colocation.

As in the DL, the intended power received by the b -th satellite antenna from the u -th user can be derived from Eq. 2 but, differently from the DL, the EIRP is a function of the UE antenna radiation pattern with respect to the angle between

TABLE I: Satellite parameters for S-band (Set-2 [14]).

Parameter	GEO	LEO	
		600 km	1200 km
a : equivalent antenna radius [m]	6	0.5	0.5
δ_{EIRP} : EIRP density [dBW/MHz]	53.5	28	34
$G_{TX,max}$: max TX gain [dBi]	45.5	24	24
$G_{RX,max}$: max RX gain [dBi]	45.5	24	24
G/T [dB/K]	14	-4.9	-4.9
N. beams	61-FFR; 127-FR3; 19-retained		

TABLE II: NB-IoT terminal parameters for S-band [19], [20].

Parameter	Value
P_{TX} : transmission power [dBm]	23
$G_{TX,max}$: max TX gain [dBi]	0
$G_{RX,max}$: max RX gain [dBi]	0
T_a : antenna temperature [K]	290
N_f : noise figure [dB]	9
Polarisation	linear
B_{DL} : DL bandwidth [kHz]	180
B_{UL} : UL bandwidth [kHz]	3.75, 15, 45, 90, 180

TABLE III: Constellation parameters for S-band [17].

Parameter	GEO	LEO	
		600 km	1200 km
Orbit type	GEO	LEO, circular	
Orbit inclination	0°	87.5°	
N_o : N. orbits	1	17	10
N_s : N. satellites (per orbit)	4	30	17
Beam diameter (at nadir) [km]	450	190	90
N_b : N. beams (per satellite)	547	127	91

the UE antenna pointing and the s -th satellite direction; for the purpose of this work the UE antenna is considered omnidirectional. While the receiving gain, $G_{RX}(\theta_u^{s,b}) = G_{max}^{(RX)} + 10 \log_{10} \Omega(\theta_u^{s,b})$, is computed according to the Bessel function in [15]; where $G_{max}^{(RX)}$ is the maximum receiving gain for the satellite.

The noise power in the UL, $N^{(UL)} = 10 \log_{10}(\kappa T B)$, depends on the satellite antenna equivalent noise temperature, T , and the user bandwidth, B . The UL CNR, $CNR_u^{(UL)}$, is thus obtained as in the DL. The overall interference in the UL, $I_u^{(UL)}$, can be easily obtained from Eq. 5 of DL case, with $I_{k,i,u}^{(UL)} = EIRP(\theta_s^j) + G_{RX}(\theta_j^{s,b}) - PL_s^j$, being the interference from the j -th interferer in the i -th beam (of k -th satellite), towards the b -th beam. Then the CIR, $CIR_u^{(UL)}$, and the CINR, $CINR_u^{(UL)}$, are thus obtained as in the DL.

For the sake of simplicity only the S-S case has been depicted, but the mathematical notation foresees the M-S scenario, *i.e.*, with $N_{sat} > 1$. In this case the angle of arrival (departure), from (towards) different satellite-beam pairs, must be computed, for both, UL and DL cases.

IV. NUMERICAL RESULTS

The link budget analysis for single- and multi-satellite scenarios, is performed by means of Monte Carlo simulations, based on the configurations reported in Tables from I to III which are derived from [14], [19], [20], and [17]. Although [14] does not explicitly consider the NB-IoT case, the selection of these parameters is based on the observation that the smaller

TABLE IV: Single- and Multi-Satellite results: CINR μ and σ in dB.

Case	GEO		LEO1200		LEO600	
	μ	σ	μ	σ	μ	σ
DL (S-S)	FFR	-5.04	1.20	-1.65	1.22	-1.65
	FR3	-3.03	1.33	5.06	0.69	5.07
DL (M-S)	FFR	-9.24	6.09	-8.13	2.81	-8.37
	FR3	-8.50	6.42	-1.20	3.16	-1.34
UL (S-S)	FFR	-4.65	1.62	-1.20	2.01	-0.82
	FR3	-2.48	1.42	5.98	1.14	8.24
UL (M-S)	FFR	-6.45	6.40	-3.81	3.56	-3.50
	FR3	-5.26	3.85	0.21	3.34	3.55

antenna size at the satellite, as it is in Set-2, is adequate also to the NB-IoT case. As a matter of fact in an IoT scenario, not only the IoT devices must be low-cost and low-energy, but it is equally important to have small, low-complexity equipment also in the space segment to reduce the cost of the infrastructure and thus the need of a small low cost antenna at the satellite. Although the parameters chosen for the constellations allow to achieve a global coverage, the actual antenna implementation that allows to obtain such a massive number of beams, could be impractical, in particular on small and cheap LEO platform. It is a fair assumption that a lower number of beams will be considered for actual implementations. Furthermore constellations with partial coverage will be probably considered for IoT services in the near future, and therefore these aspects will be subject of future studies.

Also, since NB-IoT terminals are not defined in the same 3GPP simulation set, we modified the system bandwidth in line with the NB-IoT system by choosing 180 kHz for the DL and 3.75, 15, 45, 90, 180 kHz for the UL, regardless to the adopted FR scheme, *i.e.*, Full Frequency Reuse (FFR) and Frequency Reuse 3 (FR3). For the sake of synthesis, only the results for the case with $B = 45$ kHz will be shown for the UL scenario, *i.e.*, the Narrowband Physical Uplink Shared Channel (NPUSCH) Format 1 configuration, with 3 tones allocation [20]. For what concern the UE parameters, we refer to [19] and [21], considering NB-IoT Class 3 terminals.

A. Single-satellite scenario

For S-S scenario the beams are located on the u - v plane so as to have equivalent elevation of the satellite at 45° (GEO) or at 90° (LEO) [14] from the coverage center. A variable number of tiers is considered depending on the FR scheme so as to ensure that the same number of interfering beams is considered for all scenarios; in order to properly model the overall interference experienced by each UE, the numerical results are gathered from the 19 internal beams only, which are highlighted by the thick blue line in the example in Fig. 4a. UE are deployed in the coverage on a regular grid in u - v coordinates. It shall then be noticed that, in the DL, the interference towards any UE is generated by the co-channel transmitting antennas on the satellite; thus, interference is defined by geometry, *i.e.*, it is fixed given the receiving UE location and the beam layout configuration. The only stochastic aspect to be taken into account is the shadow fading, modelled as a lognormal random variable $PL_\sigma \sim (0, \sigma^2)$ with the values of σ^2 depending on the UE's elevation angle [15]. As for the UL,

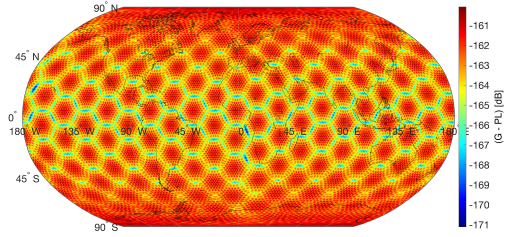


Fig. 5: Example of satellite constellation coverage (1200 km).

interference is clearly depending on the specific interfering UE locations. In this case then, both the stochastic shadow fading and the interference source location vary through Monte Carlo iterations. Furthermore the interference is not defined by geometry as in the DL, but it is impacted by the scheduling algorithm, which is assumed to be random, with one UE per beam transmitting at each iteration as it is in [14].

Figures from 6 to 8, show the CNR, CIR and CINR Cumulative Distribution Function (CDF) for the DL, while figures from 9 to 11 for the UL. Table IV provides the mean and standard deviation of the CINR for all cases. As can be seen from the results, the CINR with FFR is quite low for all scenarios; this is related to the severe interfering environment since no interference management technique is implemented. An improvement of the performance can be seen for FR3. The difference in the standard deviation between the DL and the UL scenarios is motivated by the fact that, in the DL, interference is defined by geometry, *i.e.*, the beam layout is fixed and the interfering satellite antennas are always transmitting towards their beam centers; while in the UL, a random scheduling algorithm is implemented to identify the interfering users at each time frame and, thus, an increased variability arises.

B. Multi-satellite scenario

The simulations for the M-S scenario are time-driven, *i.e.*, at each time instant the geometry of the constellation changes, thus the link budget and interference components change. Then both the satellite constellation geometry, and the stochastic shadow fading previously described, vary through Monte Carlo iterations. The UE are deployed on a regular *lat-lon* grid and the statistics are gathered from all the points of the grid. The performance analysis is then computed for the whole evolution in time of the satellite constellation, considering a uniform user deployment. For each constellation geometry, the UE are assigned to the best satellite/beam pair according to the link budget fixed terms, *i.e.*, the antenna pattern for the constellation is projected in *lat-lon* coordinates, as previously described, then the highest value of $G(\theta_s^u) - PL_{fs}$ is chosen for each UE such to identify the best serving satellite/beam pair. An example of global coverage, showing the link budget fixed terms, is depicted in Fig. 5. The minimum elevation angle considered for the UE is 10°. In the DL, the useful received signal, C (Eq. 2), is computed with respect to the best serving satellite/beam pair while the interference, I (Eq. 5), is considered from all the satellite/beam pairs visible to the UE. As opposed to the S-S scenario here the interference toward

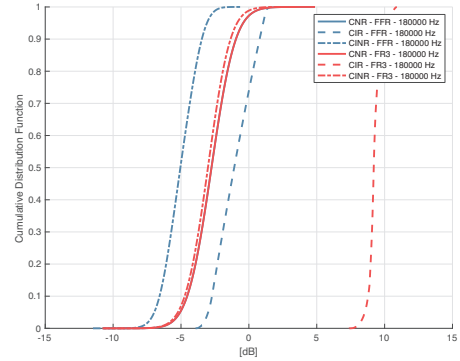


Fig. 6: Downlink link budget for GEO satellite.

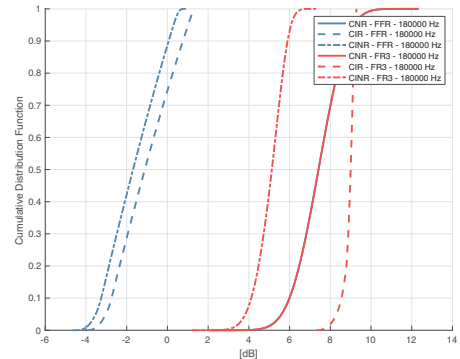


Fig. 7: Downlink link budget for LEO satellite at 1200 km.

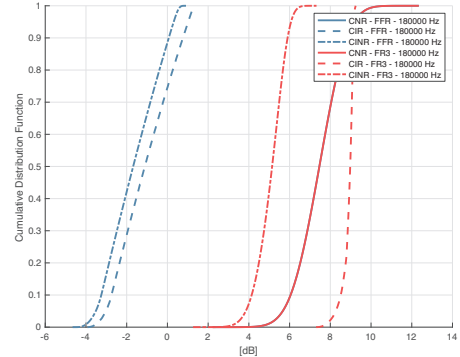


Fig. 8: Downlink link budget for LEO satellite at 600 km.

any UE is not only dependent by the beam layout geometry, but also from the satellite-UE relative positions, *i.e.*, slant range and elevation angle with respect all the constellation satellites. As for the UL, a random scheduling is performed in the same fashion of S-S scenario, such to select only one transmitting UE for each beam of every satellite. Then the interference towards all the satellite/beam pairs visible from the UE are computed, as previously described, accounting for the satellite-UE relative geometry. In this case then the interference is also impacted by the scheduling algorithm.

For the sake of synthesis, CDF graphs are not shown but a summary of the results, with mean and standard deviation of the CINR for all cases, is shown in Table IV. As it is expected the mean values of all cases are lower with respect to the link budget calibration results shown previously, while the standard deviation is higher. These results are motivated by the fact that,

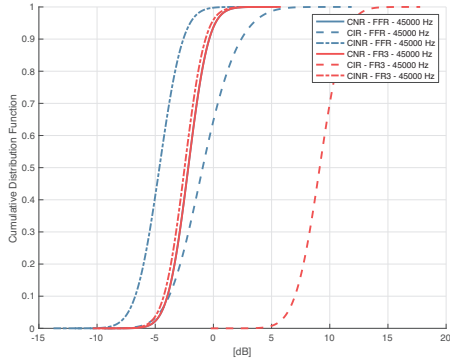


Fig. 9: Uplink link budget for GEO satellite.

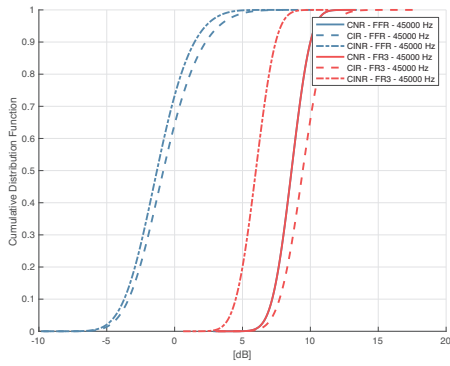


Fig. 10: Uplink link budget for LEO satellite at 1200 km.

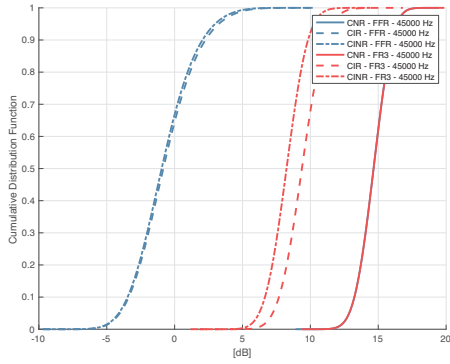


Fig. 11: Uplink link budget for LEO satellite at 600 km.

the coverage is much bigger with respect to the S-S scenario; focusing on the LEO at 600 km for example, the coverage is composed from $N_{beams} = 127$ beams, opposed to the 19 retained beams for the statistics for the S-S scenario.

V. CONCLUSIONS AND FUTURE WORKS

In this paper, we focused on a link budget analysis for NB-IoT over NTN systems, based on link budget calibration approach for S-band systems, in [14]. A detailed discussion on the current system architecture and assumptions was provided, together with a thorough description of the methodology, for both single- and multi-satellite simulations. Numerical results were reported and discussed showing that FFR schemes require the implementation of interference management techniques, while for multi-color FR schemes the link budget already provides a good performance. It is worthwhile high-

lighting that the study on NB-IoT integration in NTN is ongoing within 3GPP, so future works will target the evolution of this standardization process.

REFERENCES

- [1] Cisco, “Cisco Annual Internet Report (2018–2023).”
- [2] A. Guidotti *et al.*, “Architectures and Key Technical Challenges for 5G Systems Incorporating Satellites,” *IEEE TVT*, Mar. 2019.
- [3] A. Guidotti *et al.*, “LTE based satellite communications in LEO mega constellations,” *IJSNC*, Jul. 2019.
- [4] A. Guidotti, “Beam Size Design for New Radio Satellite Communications Systems,” *IEEE TVT*, Nov. 2019.
- [5] S. Cioni *et al.*, “On the Satellite Role in the Era of 5G Massive Machine Type Communications,” *IEEE Network*, Sep. 2018.
- [6] N. Alagha, “Satellite Air Interface Evolutions in the 5G and IoT Era,” *SIGMETRICS Perform. Eval. Rev.*, Jan. 25, 2019.
- [7] M. Inc., “RP-193235 Study on NB-IoT/eMTC support for NTN,” Dec. 2019.
- [8] M. Gineste *et al.*, “Narrowband IoT Service Provision to 5G User Equipment via a Satellite Component,” in *IEEE GC Wkshps 2017*, Dec. 2017.
- [9] O. Kodheli *et al.*, “Resource Allocation Approach for Differential Doppler Reduction in NB-IoT over LEO Satellite,” in *ASMS/SPSC 2018*, Sep. 2018.
- [10] —, “An Uplink UE Group-Based Scheduling Technique for 5G mMTC Systems Over LEO Satellite,” *IEEE Access*, 2019.
- [11] M. Conti *et al.*, “Doppler Impact Analysis for NB-IoT and Satellite Systems Integration,” in *IEEE ICC2020*, May 2020.
- [12] S. Cluzel *et al.*, “3GPP NB-IOT Coverage Extension Using LEO Satellites,” in *2018 IEEE 87th Vehicular Technology Conference (VTC Spring)*, Jun. 2018.
- [13] O. Kodheli *et al.*, “Link Budget Analysis for Satellite-Based Narrowband IoT Systems,” in *Ad-Hoc, Mobile, and Wireless Networks*, ser. Lecture Notes in Computer Science, M. R. Palattella *et al.*, Eds., 2019.
- [14] 3GPP, “TR38.821 TSG-RAN Solutions for NR to support NTN R16,” Dec. 2019.
- [15] —, “TR38.811 TSG-RAN Study on NR to support NTN R15,” Sep. 2019.
- [16] A. Guidotti *et al.*, “Non-Terrestrial Networks: Link Budget Analysis,” Oct. 26, 2019.
- [17] H. Huawei, “R1-19111858 Discussion on performance evaluation for NTN,” Nov. 2019.
- [18] J. R. Wertz *et al.*, Eds., *Space Mission Analysis and Design*, 3rd ed. 1999.
- [19] —, “R1-1903998: Discussion on link budget for NTN,” Apr. 2019.
- [20] 3GPP, “TS36.211 TSG-RAN E-UTRA and E-UTRAN Physical Channels and Modulation R16,” Mar. 2020.
- [21] —, “TR36.888 TSG-RAN Study on provision of low-cost MTC UEs based on LTE,” Jun. 2013.